Advances in Nano Research, *Vol. 15, No. 4 (2023) 295-304*
https://doi.org/10.12989/anr.2023.15.4.295

Functional graphene sheets-TiO_2 nanocomposites and their photocatalytic performance for wastewater treatment

R. Aitbelale*[1], A. Timesli**[2] and A. Sahibed-dine[1]

[1]*University of Chouaïb Doukkali, Faculty of sciences, Laboratory of Catalysis and Corrosion of Materials, El Jadida, Morocco.*
[2]*Hassan II University of Casablanca, National Higher School of Arts and Crafts (ENSAM CASABLANCA), AICSE Laboratory, 20670 Casablanca, Morocco*

(*Received March 4, 2022, Revised August 11, 2023, Accepted August 24, 2023*)

Abstract. In this paper, a powerful photocatalyst based on carbon nanocomposite is developed in order to obtain a new material applicable in water treatment and especially for the discoloration of effluents used in the textile industry. For that, TiO_2-graphene nanocomposites have been successfully synthesized by a mixture of Functionalized Graphene Sheet (FGS) and tetrachlorotitanium complexes to form FGS-TiO_2 nanocomposite. In the presence of an anionic surfactant, we used a new chemical process to functionalize graphene sheets in order to make them an excellent medium for blocking and preventing the aggregation of TiO_2 nanoparticles. The components of these nanocomposites are characterized by means of X-ray diffraction (XRD), Fourier Transform Infrared Spectroscopy (FT-IR), Scanning Electron Microscopy (SEM) and Transmission Electron Microscopy (TEM), which confirms the successful formation of the FGS-TiO_2 nanocomposite. It was found that the TiO_2 nanoparticles were dispersed uniformly on the graphene plane which possesses better charge separation capability than pure TiO_2. The FGS-TiO_2 nanocomposites exhibited higher photocatalytic activity compared to pure TiO_2 for the removal of three dyes: such as Methylene Blue (MB), Bromophenol Blue (BB) and Alizarin Red-S (AR) in water. The removal process was fast and more efficient with FGS-TiO_2 nanocomposite in daylight (in the absence of UV irradiation) compared to pure TiO_2 nanoparticles without and under UV in all pH range.
Keywords: graphene; nanocomposite; photocatalyst; tetrachlorotitanium; wastewater

1. Introduction

Nanocomposites come in several types based on their matrix and nano material phases. The development of nanocomposites also depends on their use. For exemple, Carbon nanotubes (CNTs) and graphene nanoplatelets are mainly used as reinforcing material as indicated in the literature (Zerrouki *et al*. 2021, Heidari *et al*. 2021, Al-Furjan *et al*. 2021, Bourada *et al*. 2020, El Haouzi *et al*. 2023, Aitbelale and Timesli 2023). Furthermore, other type of nanocomposites are based on the existence of porosities which can affect considerably of nanocomposites for a more efficient manufacturing of these types of materials and their technical design (Arshid *et al*. 2022). There are also sandwich nanostructures (Bendenia *et al*. 2020, Al-Furjan *et al*. 2022a, 2022b, Timesli 2023). Another type of nanocomposites based on FGS-TiO2 is studied in this paper.

Currently, TiO_2 has become the most widely used semiconductor in the photocatalytic processes. Generally, TiO_2 nanoparticles considered as the most reliable for the degradation of volatile organic compounds due to their non-toxicity, low cost, physical and chemical stability, interesting specific area and high reactivity (Goodeve and Kitchener 1938, Hashimoto *et al*. 2005, Fujishima and Honda 1972, Frank and Bard 1977, Tabatabaei 2019, Tabatabaei *et al*. 2019, Safavi *et al*. 2017). However, the use of TiO_2 nanoparticles alone poses significant problems related to water purification and waste produced after treatment (Gottschalk and Nowack 2011, Farré *et al*. 2010). Among the obstacles of using TiO_2 as a photocatalyst in the photodegradation of pollutants is its very low adsorption capacity of some dyes (Zhao *et al*. 1998) and other organic pollutants (Torimoto *et al*. 1996, Xu and Langford 1995). Thus, various approaches have been explored to extending the photocatalytic activity of TiO_2 from the ultraviolet to the visible region by modification (Kalathil *et al*. 2013, Khan *et al*. 2014) or by doping with several elements such as C, N, F, P and S (Chang *et al*. 2005). One of the most favorable way to overcome these problems is the immobilization of TiO_2 on solid support such as activated carbon (Foo and Hameed 2010), glass (Serpone *et al*. 1986), ceramic (Sabate *et al*. 1992), zeolite (Zhang *et al*. 2018), natural phosphate (Naciri *et al*. 2016) and graphene oxide (Štengl *et al*. 2013), which they give a profound advantages of straightforward recovery, preservation of morphology and the improvement of the stability. However, this support-TiO_2 bonding result generally a significant decrease in photocatalytic activity due to a decrease in accessible surface area available for reaction and a limitation in mobilization compared to the suspension of TiO_2 nanoparticles alone (Thiruvenkatachari *et al*. 2008, Cunha *et al*. 2018). However, when TiO_2 nanoparticles are assembled with powerful photocatalyst, such as

*Corresponding author, Ph.D.,
E-mail: aitbelale.rachid@yahoo.fr
**Co-corresponding author, Ph.D., Professor,
E-mail: ABDELAZIZ.TIMESLI@univh2c.ma

Copyright © 2023 Techno-Press, Ltd.

ISSN: 2287-237X (Print), 2287-2388 (Online)

graphene, this problem does not arise and the separation becomes easier (Padmanabhan *et al*. 2021). From 2004, the synthesis of graphene sheets (GS) (Novoselov *et al*. 2004) allowed to reveal the unique character electrical properties of this material, such as the electron mobility under ultrahigh vacuum (200 000 $cm^2V^{-1}s^{-1}$) (Lee *et al*. 2008). In addition, the GS nanomaterial has interesting texture, optical and thermal properties, highly flexible structure (Allen *et al*. 2010), a large specific area (2630 m^2/g) (Stoller *et al*. 2008), a high transparency (97.7% of optical transmission) (Nair *et al*. 2008), and a high thermal conductivity of about 5000 $Wm^{-1}K^{-1}$ (Balandin *et al*. 2008). Because of their unique structural and electronic properties, graphene has gained a lot of considerable attention (Tu *et al*. 2013).

Based on this observation, various researchers have tried to improve the photo-activity of TiO_2 by developing composites based on carbon allotropes. Lee *et al*. (2005) developed TiO_2 doped with multi-walled carbon nanotubes (MWCNTs). These authors hypothesized that the excited electrons can be trapped at the interface between the TiO_2 layer and MWNTs, also can be scavenged through the conductive graphitic layers. These materials were found to be very active, compared to pure TiO_2. In the Krishna works (Krishna *et al*. 2006, 2008), the addition of functionalized C60 (polyhydroxyfullerene, PHF) to the TiO_2 showed an improvement in the photocatalytic activity for dye degradation. The generation of hydroxyl radicals was detected using electron paramagnetic resonance spectroscopy and the results showed that the percentage of these radicals increased from 20% in the case of the pure TiO_2 to 60% in the presence of PHF-TiO_2. Hence, this recent work makes it possible to consider the use of these systems (C-TiO_2) in order to improve the photocatalytic performance of titanium oxide.

Compared with the C60 and CNTs (Timesli 2020, 2021), graphene has a structure sp2 hybridized carbon in two dimensions with better conductivity and large surface, it seems reasonable to consider that the TiO_2-graphene nanocomposites could be much more promising to improve photocatalytic performance of TiO_2. Furthermore, graphene is easy to produce from natural graphite (Hummers and Offeman 1958). The presence of oxygen functional groups on the surface containing the graphene oxide (GO) make it an excellent medium to block TiO2 nanocrystals (Nguyen *et al*. 2020)

The dyes are present in the effluent of serious concern, and can cause a harmful effect on humans and the environment (Banat *et al*. 1996). In addition, the color dyes are easily recognizable, even at very low concentrations, making them highly visible and undesirable. Many technologies have been devoted to the removal of dye from aquatic environments, including physical, chemical, and biological adsorption which is considered as economical and sustainable processes (Houas *et al*. 2001). The rapid development of nanotechnology sheds light on the treatment of wastewater. Nanomaterials have been studied for absorption of metal ions, dyes, and antibiotics. Although it was discovered just a few years ago, graphene and its derivatives have attracted immense research interest not only in electronics and energy fields as well as in environmental applications. For example, GO could be used for the removal of heavy metals (Zhang *et al*. 2020). In addition, the graphene composites, such as TiO_2-graphene, were used to remove pollutions and the dye (Dadvar *et al* 2017).

Herein, in this present work, we report a convenient method for the in-situ preparation of FGS/TiO_2 nanocomposite and its application in the removal of three dyes: Methylene Blue (MB), Bromophenol Blue (BB) and Alizarin Red-S (AR). Graphene Sheet (GS) was synthesized by exfoliation of Graphene oxide (GO) already prepared by modified Hummers method and functionalized by a new chemical method; thereafter titanium oxide (TiO_2) was in-situ supported on FGS. The synthesized heterogeneous photocatalyst is well characterized by XRD, FT-IR, SEM and TEM techniques. The FGS/TiO_2 nanocomposites were successfully used as an absorbent for effective degradation of the dyes compared to the TiO_2 alone. The removal process has been found to be more efficient at higher and lower pH values. Moreover, the catalyst was successfully recycled for seven times.

2. Experimental

2.1 Materials

All chemicals were obtained commercially and used without further purification. Natural graphite flakes (diameter 5-10 μm, thickness4-20 nm, layers <30 and purity >99.5 wt %) and Titanium chloride (TiCl4, 99.90%) were purchased from Sigma-Aldrich. Concentrated Sulfuric acid (H2SO4, 98%), concentrated Hydrochloric acid (HCl), concentrated Nitric acid (HNO3) and Hydrogen Peroxide (H2O2, 35%) were obtained from Fisher. Potassium Permanganate (KMnO4) was purchased from Merck. All the reagents are of analytical grade. The solutions were prepared by using pure distilled water. Characteristics and molecular structures of dyes (MB, MR and TR) are shown in Table 1.

UV-visible absorption spectra of MB, BB and AR were obtained by spectral scanning of a 100mg.L-1 solution dye (concentration 100mg.L-1) between 450 and 800 nm. The result shows that the maximum wavelengths absorption for each dyes are 663nm, 592nm and 558nm respectively.

2.2 Synthesis of graphene sheets

Graphene oxide was synthesized by the oxidation of graphite powder using Hummers method (Hummers and Offeman 1958). In a typical procedure, in a round bottom flask, between 0 and 5°C, 6g of graphite flakes and 3 g of sodium nitrate ($NaNO_3$) were mixed in 140 ml of sulfuric acid (H_2SO_4). After homogenization of the mixture, 18g of potassium permanganate ($KMnO_4$) was added slowly. The solution is kept at room temperature under constant stirring for 12 hours. Thereafter, 250mL of deionized water was added to the suspension. After that, the suspension was treated with a solution of hydrogen peroxide slowly till the

Table 1 Summary of reactor performance

Dyes name	Linear formula	Mw(g/mol)	Purity (%)	CAS
Methylene Blue	$C_{16}H_{18}ClN_3S_3H_2O$	373.90	98.0	61-73-4
Bromophenol Blue	$C_{19}H_{10}Br_4O_5S$	669.96	98.8	115-39-9
Alizarin Red S	$C_{14}H_7NaO_7S$	342.25	99.4	1934-21-0

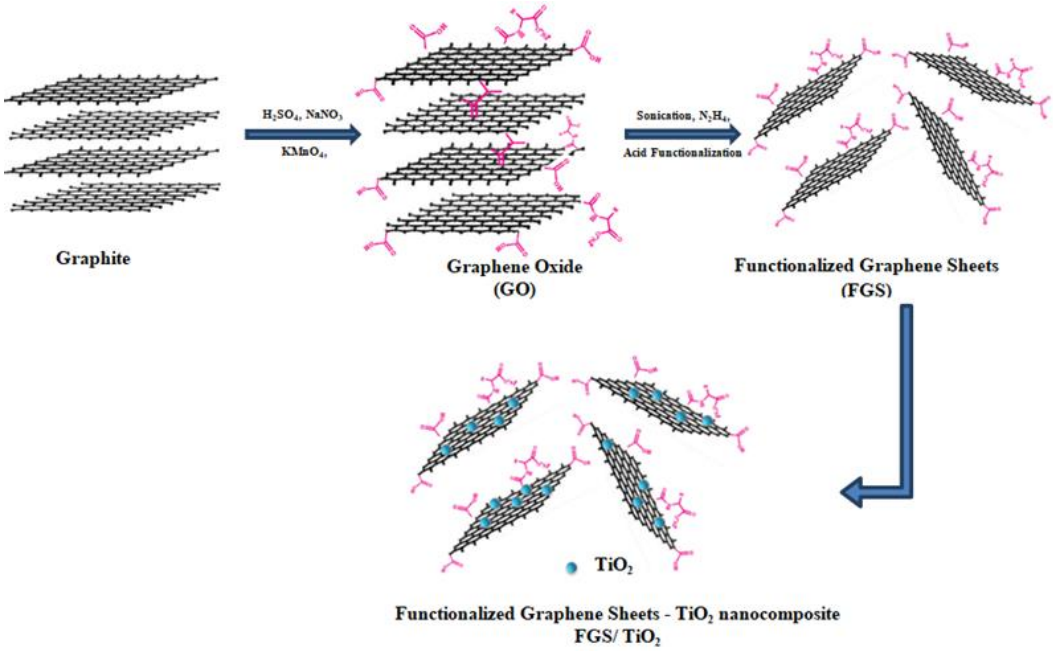

Fig. 1 Schematic representation of the synthesis of FGS-TiO_2 nanocomposites

color of the solution turned to bright yellow and then filtered. The filter is re-dispersed, washed with hydrochloric acid solution to reduce the residual manganese ions and then washed several times with distilled water until the pH of solution becomes neutral to remove residual salts and acids. The graphene oxide was obtained after filtration and drying in an oven. The exfoliation is an important step in the production of graphene nanosheets. Exfoliation techniques either in solvents or thermally at high temperature remain the two preferred synthesis routes; in the case of exfoliation in the presence of solvents, the hydrophilic nature and the large interlayer spacing of graphene oxide can make easer exfoliation in water using a mechanical treatment such as ultrasonic treatment or mechanical agitation at concentrations up to 3mg.mL^{-1}. This technique allows obtaining stable colloidal suspensions of graphene oxide nanosheets from graphene oxide. To proceed to the exfoliation step, a mass of 100mg of graphene oxide was suspended in 250mL of water in presence of 10 ml of hydrazine hydrate and dispersed by sonication for 1 hour 30 minutes. After 12 hours of heating at 100°C, the reduced graphene will be washed with distilled water several times and dried under vacuum.

2.3 Synthesis of functionalized graphene sheets

0.1g of Graphene Sheet (GS) was dispersed in a mixture of concentrated acids (0.3 g of sulfuric and nitric acids) in 10 ml of distilled water. The mixture was stirred for 24h at room temperature, after that, the suspension was treated by an equimolar amount of NaOH in distilled water (10 mL) to neutralize the residual acids and filtered. The filter is washed several times with distilled water until the pH of solution becomes neutral and treated with a solution of ethanol. The final precipitate of FGS was centrifuged, washed with H2O/ EtOH and finally dried under vacuum in an oven.

2.4 Synthesis of FGS/ TiO2 nanocomposite

The in-situ preparation of binary nanocomposite of graphene and titanium dioxide nanoparticles was prepared as follows: Under stirring, to an aqueous solution of SLES (sodium lauryl ether sulfate) 0.01M as an anionic surfactant, a solution of FGS already dispersed and ultrasonicated in absolute ethanol during an hour was slowly added. The purpose to use an anionic surfactant is to avoid the aggregation of TiO_2 nanoparticles on the graphene surface. The mixture is placed in an ultrasonic bath for 2h, stirred vigorously for 1h by a magnetic stirrer. After that, a solution of titanium tetrachloride TiC_{l4} (0.05M) was added, after 30min of stirring, a solution of ammonia (0.2M) was slowly added with constant stirring until the pH is maintained at 8. After 30 min of stirring and sonication, nitric acid (1M) is added until the pH is equal to 2. This final solution was placed in an autoclave and heated at 150°C for 3h and washed successively with ethanol and water. The product was preserved in a desiccator and calcined at 600°C for 3h

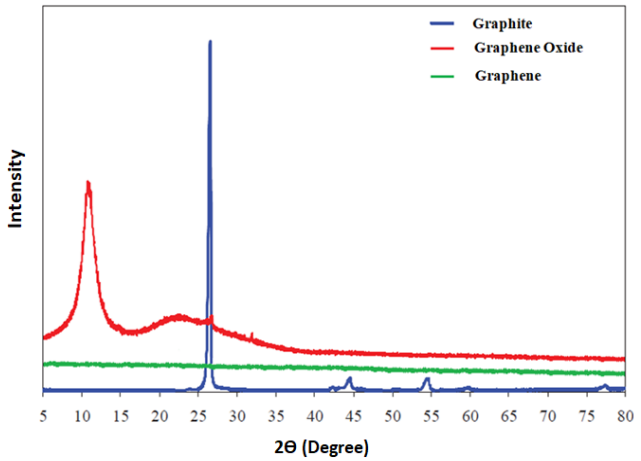

Fig. 2 XRD pattern of: (a) graphite, (b) graphene oxide and (c) graphene

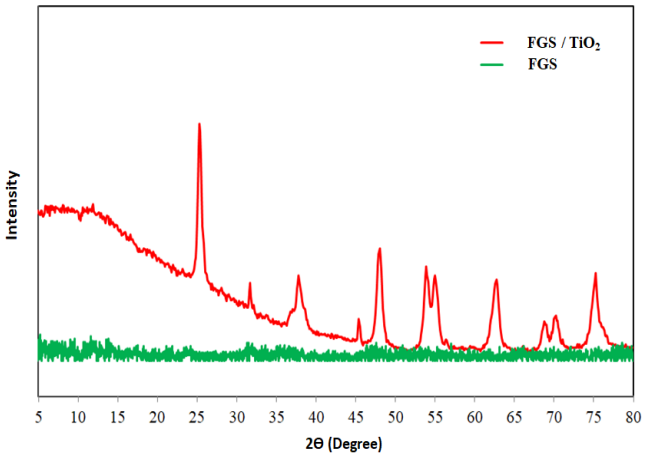

Fig. 3 XRD pattern of: (a) functionalized graphene sheets (FGS) and (b) functionalized graphene sheets-TiO2 nano-composite (FGS-TiO2)

to obtain the functionalized graphene sheets-titanium dioxide nanocomposite (FGS-TiO_2). A stepwise schematic representation of the synthesis is shown in Fig. 1.

2.5 Catalyst characterization

FT-IR spectra were used for each sample to examine the bonding interactions before and after oxidation and functionalization processes. FT-IR spectra were recorded with a FTLA2000-102 Spectrometer (commercialized by ABB Bomem Company) equipped with ATR (Attenuated Total Reflexion). The spectra are scanned between 260 and 4000 cm-1. A resolution of 4 cm-1 is considered optimal for obtaining good spectrum quality in ATR mode. The FTIR calibration is performed daily and automatically according to a procedure based on a band of water vapor absorption in the ambient air. The contact pressure of the sample on the diamond crystal is controlled manually using a fixation system which allows to optimize the contact and to have quality spectra. XRD was used to characterize the atomic arrangement of the crystalline structure. XRD spectra of graphite and graphene materials were collected using a Bruker AXS D-8 Advanced diffractometer with a copper target at the wave length of λ= 1.5406 Å, a tube voltage of 40 kV and a Bragg-Brentano geometry (Θ, 2Θ) in the range of 5-100°. SEM (Scanning electron microscopy) was used to observe the texture of graphite oxide and graphene obtained after complete exfoliation of graphite. The microstructural characterization of materials provides several informations relating to morphology, component distribution, crystallography and composition. SEM image was obtained using "Quanta 200" from FEI Company, which can achieve a resolution of 3.0 nm at voltage of 30kV. The morphology of FGS-TiO_2 nanocomposite was observed using the Transmission electron microscopy (TEM), the TEM image was obtained using Philips FEI SIRION-200 operated at 30kV for a resolution of 1.2nm.

2.6 Photocatalytic experiment

The photocatalytic activity of the three dyes (MB, BB and AR) on FGS/TiO_2 nanocoposite was evaluated in daylight without using an UV lamp. For this purpose, an amount of catalyst nanocoposite was suspended in 20 mL of each dyes solutions of initial concentration C0 (3-50 $mg.L^{-1}$). The pH of the solutions was adjusted using hydrochloric acid ($0.1mol.L^{-1}$) or sodium hydroxide ($0.1mol.L^{-1}$) solutions. The series of closed Erlenmeyer is arranged on a multi-station stirring plate at room temperature. A vigorous agitation by a magnetic bar at 250rpm allows a good contact of the solution with the catalyst. The analysis of the initial or residual dye concentration is performed by UV-Visible adsorption spectroscopy using a Micrometrics ASAP 2020.

3. Results and Discussion

3.1 X-ray diffraction study

Fig. 2 shows the XRD patterns of graphite (a), graphene oxide (b) and graphene (c). The X-ray diffraction analysis shows that graphite is well crystallized and presents a single intense line at 26.5° (inter-sheet distance: 3.4 Å) corresponding to the reticular plane (002) of graphitic carbon. After oxidation by the optimized Hummers method, the graphitic phase disappears while a new line at 10.8° accompanied by a broad band at 23° appears confirming the oxidation of graphite to graphene oxide (GO). Indeed, the inter-sheet distance increases from 3.4 Å for graphite to 8.3 Å for graphene oxide as a result of inter-sheet expansion due to the incorporation of water and oxygenated groups during the oxidation process (Mallakpour *et al*. 2014). In addition, the broad diffraction line at 23° with low intensity can be attributed to the presence of residual unexfoliated and poorly crystallized graphene sheets. After sonication, the peak of GO at 10.8° disappears; this signifies the formation of graphene sheets from graphene oxide.

Fig. 3 shows the XRD patterns of Functionalized Graphene Sheets (FGS) and FGS/TiO2 nanocomposite (FGS-TiO2). The TiO_2 nanoparticles were prepared in-situ with FGS in the presence of SLES (sodium lauryl ether sulfate) as surfactant and calcined at 600 °C. The characteristic peak appear almost show diffraction patterns corresponding to the anatase phase of TiO_2 (at 25° (101),

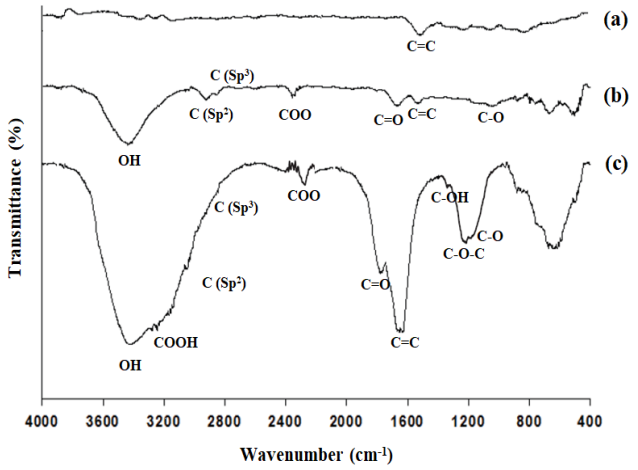

Fig. 4 FT-IR spectra of: (a) graphite, (b) graphene oxide (GO) and (c) functionalized graphene sheets (FGS)

37° (103), 48° (200), 54° (105), 55° (211), 63° (118) and 69° (116)). While, the XRD patterns of FGS- TiO_2 exhibited an uniform dispersion of TiO_2 nanoparticles on both the graphene sheets as shown in the SEM image in the SEM analysis section.

3.2 FT-IR analysis

FT-IR spectra of graphite (a), GO (b) and functionalized graphene sheets (c) are plotted in Fig. 4. Comparing to the neat graphite, the GO spectrum shows the typical vibrational modes of the oxygenated functional groups after the oxidation process: thus, the oxide functional groups give rise to a band at 1100 cm-1 corresponding to the elongation vibration mode of the C-O bond. In addition, a shoulder at 3220 cm-1 could correspond to the (O-H) vibration mode of the hydroxyl and carboxyl groups (Aitbelale *et al*. 2019, 2022b).

Aliphatic Sp2 and Sp3 C–H stretching are observed around 2920 and 2850 cm-1 respectively. whereas the bond at 1720 cm^{-1} comes from the C=O stretching groups of carboxylic acids, that prove the oxidation process, while no significant peak was found in the pure graphite. Finally, the hydroxyl groups are characterized by a band at 3420 cm^{-1} originating from the (O-H) vibration mode. While a band at 1160 cm-1 comes from a C-O-C elongation vibration. The carboxyl groups give rise to a band at 1410 cm-1attributed to COH elongation vibrations while the band at 1720 cm^{-1} comes from the C=O bond elongation vibration mode.

Finally, the hydroxyl groups are characterized by a band at 3420 cm^{-1} originating from the (O-H) vibration mode. Other vibrational bands can also be detected at 1640 cm-1 (vibration (C=C)) and at 2850 and 2920 cm^{-1} (C-H elongation vibration of sp3 and sp2 species respectively).

Concerning the functionalization of the graphene sheets, we noticed that the main characteristic bands of the GO are still present in the FGS but with a higher intensity and, also, a slight shift to higher values of the wavenumbers, which allows observing other new bonds, especially at lower wavenumbers. The bands at 1396 cm-1 and at about 1080 cm-1 characterize respectively (C-O-O) and (C-O) vibrations. The presence of a broad band around 3420 cm^{-1} attributed to the (OH) stretching bands of hydroxyl and carboxylic acid proved the successful functionalization process by the acid mixture.

3.3 SEM analysis

Fig. 5 shows the SEM images of graphene oxide (GO) graphene and TiO_2 nanoparticles in different magnifications. Compared to GO (Fig. 5(a)), graphene (Fig. 5(b)) reveal a very thin layers due to the exfoliation process of GO. The remarkable decrease in the thickness of layers after exfoliation can be attributed to the elimination of inter-laminar interactions between the basal graphene layers, which subsequently results the appearance of single graphene sheets. Furthermore, graphene shows a sheet-like structure with smooth surface compared to the GO morphology.

Concerning the TiO_2 nanoparticles (Fig. 5(c)) the direct synthesis method of TiO_2 nanoparticles allows having different size of TiO_2 anatase form. The TiO_2 nanoparticles tend to agglomerate at the end of this method even if the sizes are lower than 20nm. This among the causes conducted to develop a functionalization process in presence of a surfactant.

3.4 Transmission electron microscopic analysis

Generally, the property improvement of FGS-TiO_2 nanocomposites is strongly related to the size of TiO_2 nanoparticles and to their dispersion form on graphene layers. Thus, transmission electron microscopy (TEM) can provide additional information on the dispersion quality of graphene nano-sheets and their interaction with TiO_2.

TEM images of 1% FGS-3% TiO_2 nanocomposites are shown in Fig. 6. The TEM images of FGS-TiO_2 nanocomposites are presented in Figs. 6(a)-(d) while the Fig. 6(e) shows the TEM image of non-functionalized graphene-TiO_2 nanocomposites. The first images show the presence of large graphene sheets, and at high magnification confirm that the TiO_2 nanoparticles are very well dispersed on the FGS sheets and retain their morphology. The diameter of TiO_2 nanoparticles is about 10-20 nm while in the case of using non-functionalized graphene (Fig. 6(e)), TiO_2 nanoparticles appear as aggregates suggesting that the graphene-TiO2 interaction remains partially ineffective to disperse TiO_2. This demonstrates that the functionalization of graphene influences strongly the TiO_2 nanoparticles dispersion.

3.5 Photocatalytic activity

The photocatalytic efficiency of FGS-TiO_2 nano-composite was evaluated under daylight for aqueous solutions of MB, BB and AR dyes. A stock solution of each dye at concentrations of 1000 mg. l-1 was prepared by mixing an appropriate amount of dye with distilled water. The stock solution was suitably diluted by distilled water to prepare the different desired initial concentration C_0. Thereafter, an amount of catalyst was added in 20mL of

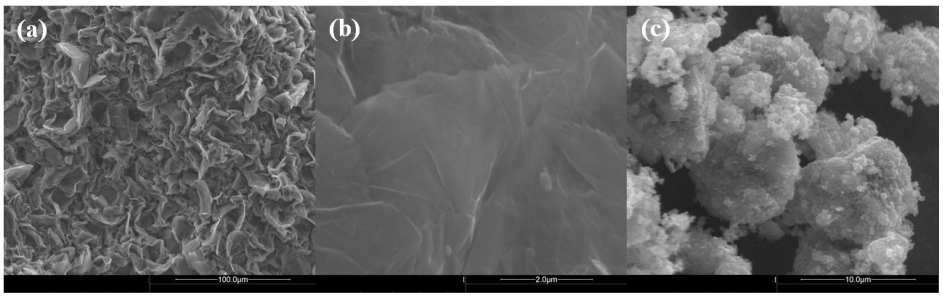

Fig. 5 SEM images of: (a) graphene oxide (GO), (b) graphene and (c) TiO2 nanoparticles

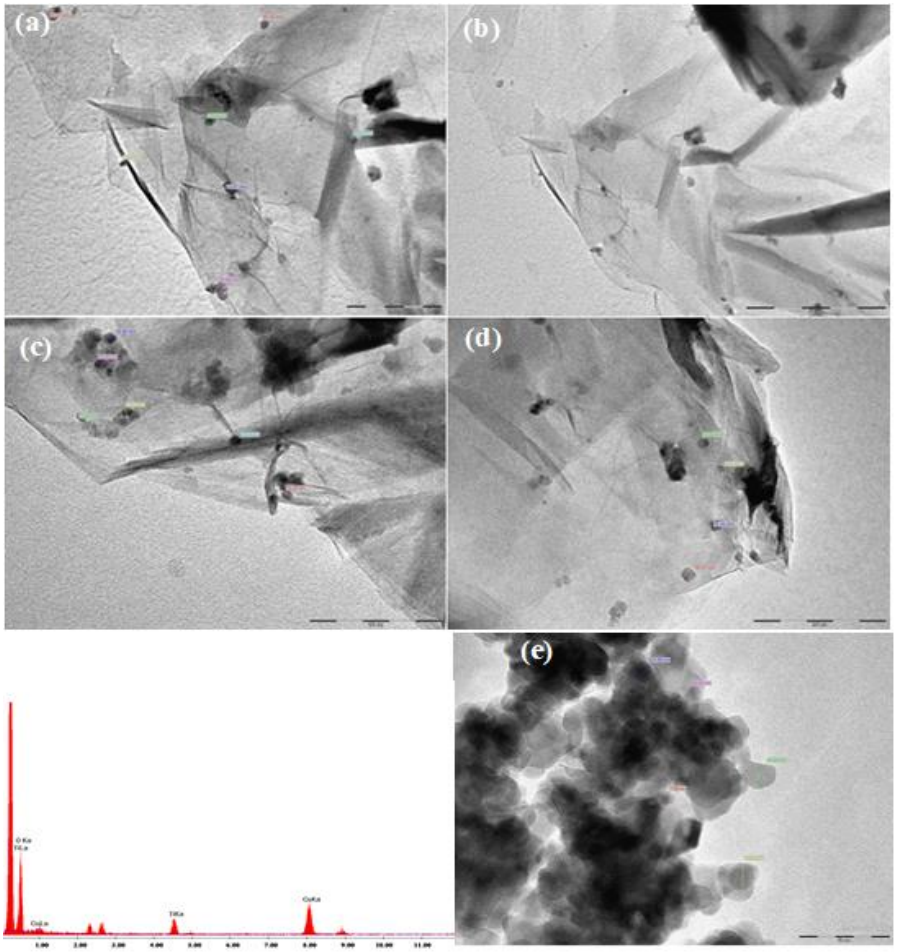

Fig. 6 TEM images of: (a)-(d) FGS-TiO_2 and (e) non-functionalized graphene-TiO_2 nanocomposites

prepared solution at room temperature without using UV irradiation. The samples were collected every 15 minutes to measure the rate of degradation.

The determination of kinetics of the reactions and the influence of some physicochemical parameters on the kinetics is an important step in the design and optimization of industrial systems. The study of the kinetics of photocatalytic reaction of the dye as a function of the initial concentration was carried by varying the initial concentrations of dyes (10-50mg.L^{-1}) at pH initial. When the materials are added (FGS, TiO_2 or FGS-TiO_2 nano-composites) in the solution, the time required for decolonization depends on the initial concentration. Furthermore, higher initial dye concentration takes much longer time to be decolorized. Photocatalysis with our materials, especially FGS and FGS-TiO_2, is a suitable system for the degradation of pollutants in very low concentrations in aqueous medium.

The kinetics degradation of Methylene Blue (MB), Bromophenol Blue (BB) and Alizarin Red-S (AR) in water is done over time by colorimetric analysis. In Fig. 7, we present the results of degradation of methylene blue using: photolysis (UV irradiation only), photocatalysis (using FGS-TiO_2 + UV irradiation,) and in daylight (using FGS-TiO_2 without UV irradiation). The results obtained showed the efficiency of graphene alone in absence of UV irradiation in the degradation of the dye. This shows that irradiation by ultraviolet radiation is not important in the presence of graphene and its derivatives. Fig. 8 shows the results of the kinetics study of (1) MB, (2) BB and (3) AR

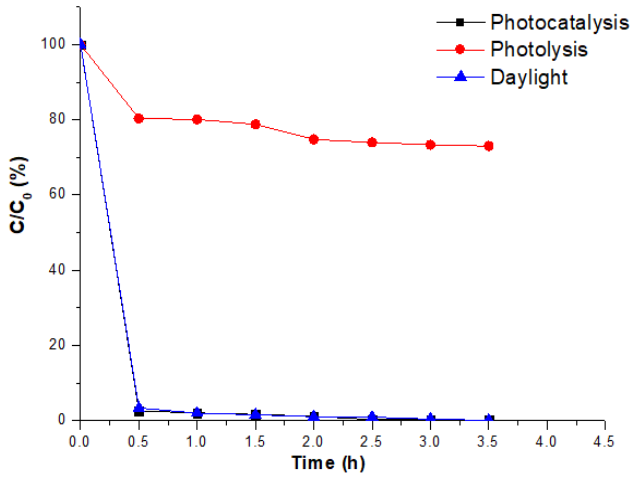

Fig. 7 Kinetics degradation of Methylene Blue using: photolysis (UV irradiation only), photocatalysis (using FGS-TiO_2 + UV irradiation,) and in daylight (using FGS-TiO_2 without UV irradiation)

dyes photodegradation from aqueous solutions with: pure FGS, FGS-TiO_2 (without UV irradiation) and pure TiO_2 nanoparticles (with UV irradiation). A significant degradation is observed at the first contact between the FGS and FGS-TiO_2 for each dye, but when using pure TiO_2 nanoparticles alone, a weak degradation was noticed which means that the TiO_2 nanocomposite is not an efficient catalyst for the photodegradation compared to the FGS and FGS-TiO_2 nanocomposite. On the other hand, compared to the pure FGS, the rate of decomposition enhanced significantly when using the FGS-TiO_2 nanocomposite. In other word, the use of FGS-TiO_2 nanocomposite shows effectiveness degradation much better than that observed when using the pure FGS or pure TiO_2 nanoparticles.

A possible explanation is that the low degradation rate shown by pure TiO_2 powder is essentially due to the absence of electron peer generation, that mean the absence of UV light irradiation. The improvement in photocatalytic activity in presence of FGS is probably due to synergistic effect between FGS and TiO_2 which leads to: (1) an enhancement in the surface area by providing the active sites for redox reactions; (2) an enhancement use of visible light instead of using ultraviolet; (3) a decrease in global exciton recombination, due to high electron transport on the graphene surface (Zhang *et al*. 2010, Liang *et al*. 2012). Fig. 9 proposes a mechanism explaining the synergistic effect between FGS and TiO_2. Under visible light irradiation, the photocatalytic surface of the FGS and TiO_2 matrix produces photogenerated electrons. The photo-promoted electrons are injected to the aromatic structure of FGS from the conduction band of TiO_2, due to the positive position of its Fermi level, which makes FGS like an electron reservoir (Xia *et al*. 2019). These electrons, which are present on the surface of FGS, react with dissolved oxygen or adsorbed oxygen to form superoxide radicals and participate in the photocatalytic process. Moreover, the mobility of charge carriers also promotes electron transfer and thus improves the overall efficiency of the various photocatalytic applications.

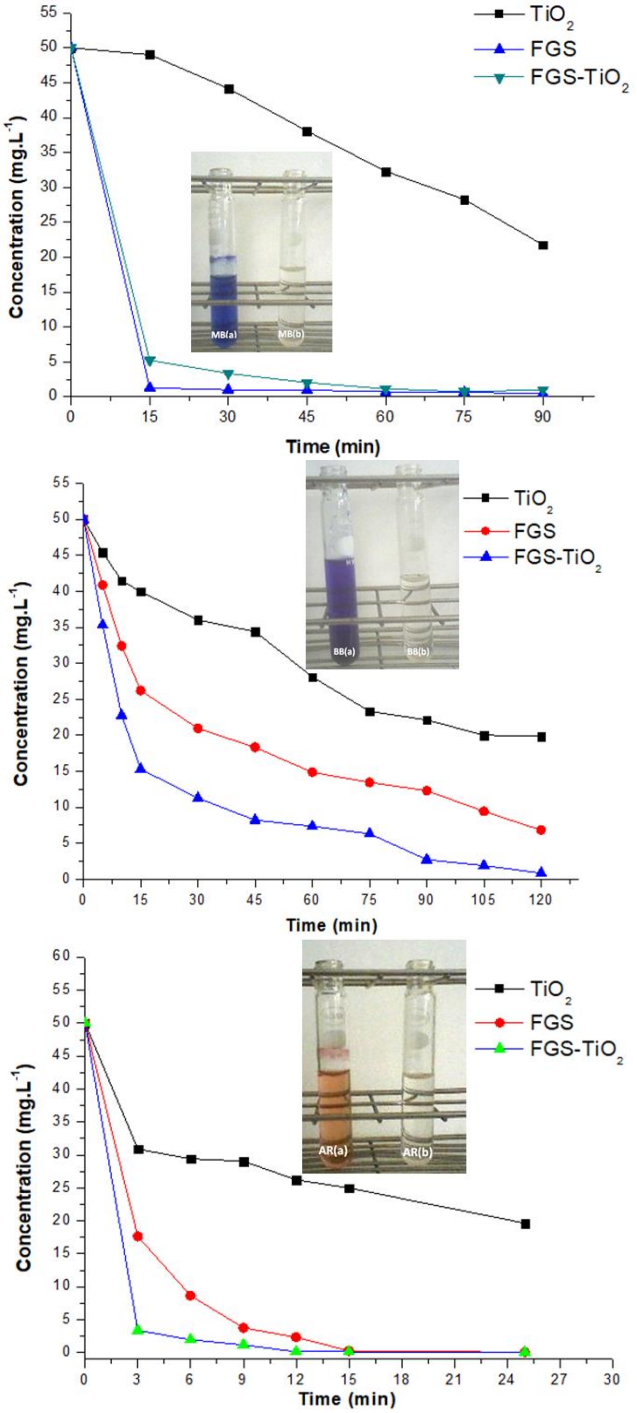

Fig. 8 Kinetic study of the degradation of various organic pollutants: (1) Methylene Blue (MB), (2) Bromophenol Blue (BB) and (3) Alizarin Red-S (AR) in water with images (a) before and (b) after degradation process

Furthermore, the electron-hole pairs would be generated and separated from the FGS- TiO_2 matrix under the effect of the congestion created by the electronic charge. Then, the generated electrons would migrate to the conduction band generated electrons would migrate to the conduction band leading to the formation of the same number of holes in the valence band. These holes would be used to form a superoxide anion radical $O_2^{\cdot-}$ when the conduction band

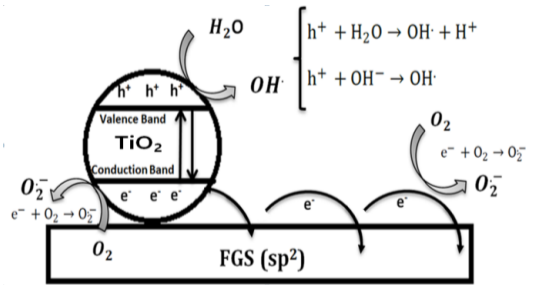

Fig. 9 Hypothetical catalytic reactions with TiO_2 supported FGS for degradation process of dyes.

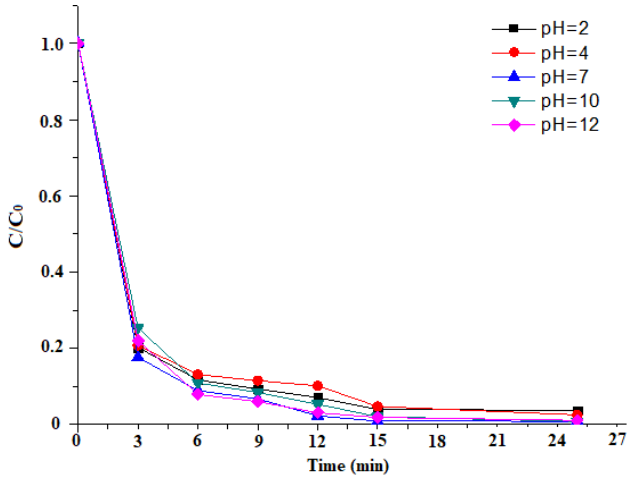

Fig. 10 Kinetics of MB photodegradation from aqueous solutions at different pH by FGS-TiO_2 nanocomposite

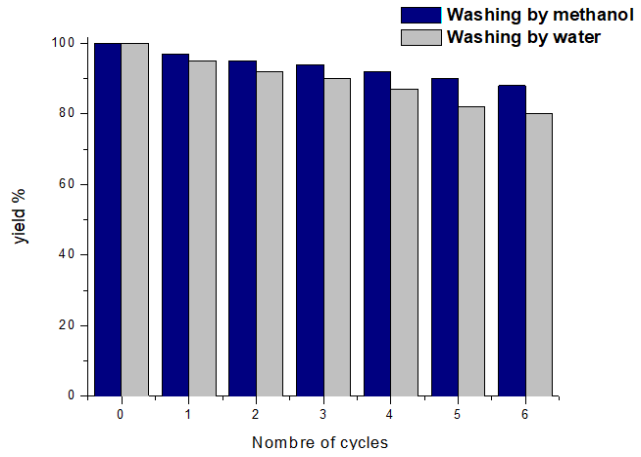

Fig. 11 Kinetics of MB dye photodegradation from aqueous solutions at different pH values by FGS-TiO_2 nanocomposite

electron reacts with O_2 which oxidize the organic compounds according to the Eq. (1).

$$\vec{B} = B_x\vec{e_x} + B_y\vec{e_y} \quad (1)$$

The valence band hole reacts with the adsorbed water or hydroxyl anions to produce hydrogen peroxide (Eq. (2)):

$$h^+ + H_2O \rightarrow OH^{\cdot} + H^+ \quad (2)$$

$$h^+ + OH^- \rightarrow OH^{\cdot} \quad (3)$$

These further splits and produces hydroxyl radicals (Eq. (3)), which is a powerful oxidizing agent and attacks organic molecules adsorbed onto the catalyst present in solution.

The pH is an important factor in any study of adsorption and degradation. This parameter characterizes the waters and its value will depend on the origin of the effluent. Processing technique to be adopted will depend strongly on the pH value. That is why, in any study on the adsorption optimization, the adsorption capacity with pH is unavailable. In our study, we monitored the effect of pH on adsorption for an initial concentration of 50mg.L^{-1}. The acidification was carried out by adding a few drops of hydrochloric acid (0.1 mol.L^{-1}). The sodium hydroxide (0.1 mol.L^{-1}) was used to make the pH basic. The results obtained (i.e. degradation of methylene blue (50mg.L^{-1})) in presence of FGS-TiO_2 (1%) are shown in Fig. 10.

The curves in Fig. 10 show a rapid decrease in dye concentration in both acidic and basic environments. We can therefore conclude that the molecular form is more retentive than the anionic form. This shows that the degradation of organic pollutants by our nanocomposites is not influenced by the hydrophilic or hydrophobic character of organic compounds. Our materials present the advantage to be reusable after washing with methanol or water. Fig. 11 shows that the catalytic activity of FGS-TiO2 remains almost unchanged after seven cycles.

4. Conclusions

The graphene-TiO_2 hybrid material was investigated for its catalytic photodegradation efficiency concerning three organic dyes, namely Methylene Blue (MB), Bromophenol Blue (BB), and Alizarin Red-S (AR), which were utilized as representative models of organic pollutants present in wastewater. This investigation was aimed at the advancement of a novel generation of TiO_2-based nanocomposites incorporating functionalized graphene sheets. In order to achieve optimal dispersion of TiO_2 nanoparticles, ionic surfactants were introduced. The incorporation of TiO_2 into the FGS structure exhibited a positive impact on their intrinsic photodegradation performance. Notably, a substantial enhancement in photocatalytic activity was discerned in materials containing FGS-TiO_2 compared to individual FGS or TiO_2 components. This observed enhancement is largely attributed to the synergistic interplay between graphene and TiO_2.

References

Allen, M.J., Tung, V.C. and Kaner, R.B. (2010), "Honeycomb carbon: A review of graphene", *Chem. Rev.*, **110**, 132-145. https://doi.org/10.1021/cr900070d

Aitbelale, R. and Timesli, A. (2023), "Effect of functionalized graphene addition on mechanical and thermal properties of high density polyethylene", *J. Polym. Eng.*, **43**(4), 343-353. https://doi.org/10.1515/polyeng-2022-0200

Aitbelale, R., Abala, I., M'Hamdi Alaoui, F.E., Sahibed-dine, A., Rujas, N.M. and Aguilar, F. (2019a), "Characterization and

determination of thermodynamic properties of waste cooking oil biodiesel: Experimental, correlation and modeling density over a wide temperature range up to 393.15 and pressure up to 140 MPa", *Fluid Phase. Equilibr*., **497**, 87-96. https://doi.org/10.1016/j.fluid.2019.06.003

Aitbelale, R., Chhiti, Y., M'Hamdi Alaoui, F.E., Sahibed-dine, A., Rujas, N.M. and Aguilar, F. (2019b), "High-pressure soybean oil biodiesel density: experimental measurements, correlation by Tait equation, and perturbed chain SAFT (PC-SAFT) modeling", *J. Chem. Eng. Data*., **64**(9), 3994-4004. https://doi.org/10.1021/acs.jced.9b00391

Al-Furjan, M.S.H., Habibi, M., Ni, J., Jung, D. and Tounsi, A. (2022a), "Frequency simulation of viscoelastic multi-phase reinforced fully symmetric systems", *Eng. Comput.*, **38**, 3725-3741. https://doi.org/10.1007/s00366-020-01200-x

Al-Furjan, M.S.H., Habibi, M., Jung, D.w., Sadeghi, S., Safarpour, H., Tounsi, A. and Chen, G. (2022b), "A computational framework for propagated waves in a sandwich doubly curved nanocomposite panel", *Eng. Comput*., **38**, 1679-1696. https://doi.org/10.1007/s00366-020-01130-8

Arshid, E., Khorasani, M., Soleimani-Javid, Z., Amir, S. and Tounsi, A, (2022), "Porosity-dependent vibration analysis of FG microplates embedded by polymeric nanocomposite patches considering hygrothermal effect via an innovative plate theory", *Eng. Comput*., **38**, 4051-4072. https://doi.org/10.1007/s00366-021-01382-y

Al-Furjan, M.S.H., Habibi, M., Ghabussi, A., Safarpour, H., Safarpour, M. and Tounsi, A. (2021), "Non-polynomial framework for stress and strain response of the FG-GPLRC disk using three-dimensional refined higher-order theory", *Eng. Struct*., **228**, 111496. https://doi.org/10.1016/j.engstruct.2020.111496.

Aitbelale, R., Abala, I., M'Hamdi Alaoui, F.E., Sahibed-dine, A., Rujas, N.M. and Aguilar, F. (2019), "Characterization and determination of thermodynamic properties of waste cooking oil biodiesel: Experimental, correlation and modeling density over a wide temperature range up to 393.15 and pressure up to 140 MPa", *Fluid Phare. Equilibr*., **497**, 87-96. https://doi.org/10.1016/j.fluid.2019.06.003

Bendenia N., Zidour M., Bousahla A.A., Bourada F., Tounsi A.D., Benrahou KH, Bedia, E.A.A. Mahmoud, S.R. and Tounsi, A. (2020), "Deflections, stresses and free vibration studies of FG-CNT reinforced sandwich plates resting on Pasternak elastic foundation", *Comput. Concr*., **25-26**(3), 213-226. https://doi.org/10.12989/CAC.2020.26.3.213

Bourada, F., Bousahla, A.A., Tounsi, A.D., Bedia, E.A. A, Mahmoud, S.R., Benrahou, K.H. and Tounsi, A. (2020), "Stability and dynamic analyses of SW-CNT reinforced concrete beam resting on elastic-foundation", *Comput. Concr*., **25**(6), 485-495. https://doi.org/10.12989/cac.2020.25.6.485

Balandin, A.A., Ghosh, S., Bao, W., Calizo, I., Teweldebrhan, D., Miao, F. and Lau, C.N. (2008), "Superior thermal conductivity of single-layer graphene", *Nano Lett.*, **8**, 902-907. https://doi.org/10.1021/nl0731872

Banat, I.M., Nigam, P., Singh, D. and Marchant, R. (1996), "Microbial decolorization of textile-dyecontaining effluents: A review", *Bioresour. Technol*., **58**, 217-227. https://doi.org/10.1016/S0960-8524(96)00113-7

Chang, J.T., Lai, Y.F. and He, J.L. (2005), "Photocatalytic performance of chromium or nitrogen doped arc ion plated-TiO2 films", *Surf. Coat. Technol*., **200**, 1640-1644. https://doi.org/10.1016/j.surfcoat.2005.08.118

Cunha, D.L., Kuznetsov, A., Achete, C.A., da Hora Machado, A.E. and Marques, M. (2018), "Immobilized TiO2 on glass spheres applied to heterogeneous photocatalysis: Photoactivity, leaching and regeneration process", *Peer J*., **6**, 4464. https://doi.org/10.7717/peerj.4464

Dadvar, E., Kalantary, R.R., Ahmad Panahi, H. and Peyravi, M. (2017), "Efficiency of polymeric membrane graphene oxide-TiO_2 for removal of azo dye", *J. Chem*., **2017**, 1-13. https://doi.org/10.1155/2017/6217987

El Haouzi, A., Belaasilia, Y. and Timesli, A. (2023), "Analytical modeling of buckling of carbon nanotubes reinforced sandwich-structured composite shells resting on elastic foundations", *Iran J. Sci. Technol. Trans. Mech. Eng*., 1-13. https://doi.org/10.1007/s40997-022-00582-1

Foo, K.Y. and Hameed, B.H. (2010), "Decontamination of textile wastewater via TiO_2/activated carbon composite materials", *Adv. Colloid Interf. Sci*., **159**, 130-143. https://doi.org/10.1016/j.cis.2010.06.002

Fujishima, A. and Honda, K. (1972), "Electrochemical photolysis of water at a semiconductor electrode", *Nature*, **238**, 37-38. https://doi.org/10.1038/238037a0

Frank, S.N. and Bard, A.J. (1977), "Heterogeneous photocatalytic oxidation of cyanide ion in aqueous solutions at titanium dioxide powder", *J. Am. Chem. Soc*., **99**, 303-304. https://doi.org/10.1021/ja00443a081

Farré, M., Pérez, S., Gajda-Schrantz, K., Osorio, V., Kantiani, L., Ginebreda, A. and Barceló, D. (2010), "First determination of C60 and C70 fullerenes and N-methylfulleropyrrolidine C60 on the suspended material of wastewater effluents by liquid chromatography hybrid quadrupole linear ion trap tandem mass spectrometry", *J. Hydrol*., **383**, 44-51. https://doi.org/10.1016/j.jhydrol.2009.08.016

Goodeve, C.F. and Kitchener, J.A. (1938), "The mechanism of photosensitisation by solids", *J. Chem. Soc. Faraday Trans*., **34,** 902-908. https://doi.org/10.1039/TF9383400902

Gottschalk, F. and Nowack, B. (2011), "The release of engineered nanomaterials to the environment", *J. Environ. Monit*, **13**, 1145-1155. https://doi.org/10.1039/C0EM00547A

Heidari, F., Taheri, K., Sheybani, M., Janghorban, M. and Tounsi, A. (2021), "On the mechanics of nanocomposites reinforced by wavy/defected/aggregated nanotubes", *Steel Compos. Struct*., **38**(5), 533-545. https://doi.org/10.12989/scs.2021.38.5.533

Hashimoto, K., Irie, H., and Fujishima, A. (2005), "TiO2 photocatalysis: A historical overview and future prospects", *Japan. J. Appl. Phys*, **44**, 8269. https://doi.org/10.1143/JJAP.44.8269

Houas, A., Lachheb, H., Ksibi, M., Elaloui, E., Guillard, C. and Herrmann, J.M. (2001), "Photocatalytic degradation pathway of methylene blue in water", *Appl. Catal. B*, **31**, 145-157. https://doi.org/10.1016/S0926-3373(00)00276-9

Hummers, W.S. and Offeman, R.E. (1958), "Preparation of graphitic oxide", *J. Am. Chem. Soc*., **80**, 1339-1339. https://doi.org/10.1021/ja01539a017

Krishna, V., Noguchi, N., Koopman, B. and Moudgil, B. (2006), "Enhancement of titanium dioxide photocatalysis by water-soluble fullerenes", *J. Colloid Interface Sci*., **304**, 166-171. https://doi.org/10.1016/j.jcis.2006.08.041

Krishna, V., Yanes, D., Imaram, W., Angerhofer, A., Koopman, B. and Moudgil, B. (2008), "Mechanism of enhanced photocatalysis with polyhydroxy fullerenes", *Appl. Catal. B*, **79**, 376-381. https://doi.org/10.1016/j.apcatb.2007.10.020

Kalathil, S., Mansoob Khan, M., Ansari, S.A., Lee, J. and Cho, M.H. (2013), "Band gap narrowing of titanium dioxide (TiO_2) nanocrystals by electrochemically active biofilms and their visible light activity", *Nanoscale*, **5**, 6323-6326. https://doi.org/10.1039/C3NR01280H

Khan, M.M., Ansari, S.A., Pradhan, D., Omaish Ansari, M., Han, D.H., Lee, J. and Cho, M.H. (2014), "Band gap engineered TiO2 nanoparticles for visible light induced photoelectron-chemical and photocatalytic studies", *J. Mater. Chem. A*., **2**, 637-644. https://doi.org/10.1039/C3TA14052K

Liang, Y.T., Vijayan, B.K., Lyandres, O., Gray, K.A. and Hersam,

M.C. (2012), "Effect of dimensionality on the photocatalytic behavior of carbonetitania nanosheet composites: charge transfer at nanomaterial interfaces", *J. Phys. Chem. Lett.*, **3**, 1760-1765. https://doi.org/10.1021/jz300491s

Lee, S.H., Pumprueg, S., Moudgil, B. and Sigmund, W. (2005), "Inactivation of bacterial endospores by photocatalytic nanocomposites", *Colloids Surf. B*, **40**, 93-98. https://doi.org/10.1016/j.colsurfb.2004.05.005

Lee, C., Wei, X., Kysar, J.W. and Hone, J. (2008), "Measurement of the elastic properties and intrinsic strength of monolayer graphene", *Science*, **321**, 385-388. https://doi.org/10.1126/science.1157996

Mallakpour, S., Abdolmaleki, A. and Borandeh, S. (2014), "Covalently functionalized graphene sheets with biocompatible natural amino acids", *Appl. Surf. Sci.*, **307**, 533-542. https://doi.org/10.1016/j.apsusc.2014.04.070

Naciri, N., Farahi, A., Rafqah, S., Nasrellah, H., El Mhammedi, M. A., Lançar, I. and Bakasse, M. (2016) "Effective photocatalytic decolorization of indigo carmine dye in Moroccan natural phosphate-TiO2 aqueous suspensions", *Opt. Mater.*, **52**, 38-43. https://doi.org/10.1016/j.optmat.2015.12.011

Novoselov, K.S., Geim, A.K., Morozov, S.V., Jiang, D.E., Zhang, Y., Dubonos, S.V. and Firsov, A.A. (2004), "Electric field effect in atomically thin carbon films", *Science*, **306**, 666-669. https://doi.org/10.1126/science.1102896

Nguyen, K.D.V. and Vo, K.D.N. (2020), "Magnetite nanoparticles-TiO2 nanoparticles-graphene oxide nanocomposite: Synthesis, characterization and photocatalytic degradation for Rhodamine-B dye", *AIMS Mater. Sci.*, **7**, 288-301. https://doi.org/10.3934/matersci.2020.3.288

Nair, R.R., Blake, P., Grigorenko, A.N., Novoselov, K.S., Booth, T.J., Stauber, T., MR Peres, N.M.R. and Geim, A.K. (2008), "Fine structure constant defines visual transparency of graphene", *Science*, **320**, 1308-1309. https://doi.org/10.1126/science.1156965

Štengl, V., Bakardjieva, S., Grygar, T.M., Bludská, J. and Kormunda, M. (2013), "TiO2-graphene oxide nanocomposite as advanced photocatalytic materials", *Chem. Cent. J.*, **7**, 1-12. https://doi.org/10.1186/1752-153X-7-41

Serpone, N., Borgarello, E., Harris, R., Cahill, P., Borgarello, M. and Pelizzetti, E. (1986), "Photocatalysis over TiO2 supported on a glass substrate", *Sol. Energy Mater.*, **14**, 121-127. https://doi.org/10.1016/0165-1633(86)90070-5

Sabate, J., Anderson, M.A., Aguado, M.A., Giménez, J., Cervera-March, S. and Hill Jr, C.G. (1992), "Comparison of TiO2 powder suspensions and TiO2 ceramic membranes supported on glass as photocatalytic systems in the reduction of chromium (VI)", *J. Mol. Catal.*, **71**, 57-68. https://doi.org/10.1016/0304-5102(92)80007-4

Safavi, B., Asadollahfardi, G. and Darban, A.K. (2017), "Cyanide removal simulation from wastewater in the presence of titanium dioxide nanoparticles", *Adv. Nano Res.*, **5**(1), 27-34. https://doi.org/10.12989/anr.2017.5.1.027

Stoller, M.D., Park, S., Zhu, Y., An, J. and Ruoff, R.S. (2008), "Graphene-based ultracapacitors", *Nano Lett.*, **8**, 3498-3502. https://doi.org/10.1021/nl802558y

Tu, W., Zhou, Y. and Zou, Z. (2013), "Versatile graphene-promoting photocatalytic performance of semiconductors: Basic principles, synthesis, solar energy conversion, and environmental applications", *Adv. Funct. Mater.*, **23**, 4996-5008. https://doi.org/10.1002/adfm.201203547

Torimoto, T., Ito, S., Kuwabata, S. and Yoneyama, H. (1996), "Effects of adsorbents used as supports for titanium dioxide loading on photocatalytic degradation of propyzamide", *Environ. Sci. Technol.*, **30**, 1275-1281. https://doi.org/10.1021/es950483k

Thiruvenkatachari, R., Vigneswaran, S. and Moon, I.S. (2008), "A review on UV/TiO2 photocatalytic oxidation process", *Korean J. Chem. Eng.*, **25**, 64-72. https://doi.org/10.1007/s11814-008-0011-8

Timesli, A. (2020), "Buckling analysis of double walled carbon nanotubes embedded in Kerr elastic medium under axial compression using the nonlocal Donnell shell theory", *Adv. Nano Res.*, **9**(2), 69-82. https://doi.org/10.12989/anr.2020.9.2.069

Timesli, A. (2021), "A cylindrical shell model for nonlocal buckling behavior of CNTs embedded in an elastic foundation under the simultaneous effects of magnetic field, temperature change, and number of walls", *Adv. Nano Res.*, **11**(6), 581-593. https://doi.org/10.12989/anr.2021.11.6.581

Timesli, A. (2023), "Analytical modeling of buckling of carbon nanotubes reinforced sandwich-structured composite shells resting on elastic foundations", *Gazi Univ. J. Sci*, **36**(4), 1700-1720. https://doi.org/10.35378/gujs.998265

Tabatabaei, J. (2019), "The effect of TiO2 nanoparticles in reduction of environmental pollution in concrete structures", *Adv. Concr. Constr.*, **7**(2), 127-129. https://doi.org/10.12989/acc.2019.7.2.127

Tabatabaei, J., Nourbakhsh, S.H. and Siahkar, M. (2019), "Mixture rule for studding the environmental pollution reduction in concrete structures containing nanoparticles", *Coupled Syst. Mech.*, **9**, 281-287. https://doi.org/10.12989/csm.2020.9.3.281

Xu, Y. and Langford, C.H. (1995), "Enhanced photoactivity of a Titanium(IV) Oxide supported on ZSM5 and Zeolite A at low coverage", *J. Phys. Chem.*, **99**, 11501-11507. https://doi.org/10.1021/j100029a031

Xia, Y., Cheng, B., Fan, J., Yu, J. and Liu, G. (2019), "Unraveling photoexcited charge transfer pathway and process of CdS/graphene nanoribbon composites toward visiblelight photo-catalytic hydrogen evolution", *Small*, **15**, 1902459. https://doi.org/10.1002/smll.201902459

Zhao, J., Wu, T., Wu, K., Oikawa, K., Hidaka, H. and Serpone, N. (1998), "Photoassisted degradation of dye pollutants. 3. degradation of the cationic dye rhodamine B in aqueous anionic surfactant/TiO_2 dispersions under visible light irradiation: Evidence for the need of substrate adsorption on TiO_2 particles", *Environ. Sci. Technol.*, **32**, 2394-2400. https://doi.org/10.1021/es9707926

Zhang, G., Song, A., Duan, Y. and Zheng, S. (2018), "Enhanced photocatalytic activity of TiO2/zeolite composite for abatement of pollutants", *Micropor. Mesopor. Mater.*, **255**, 61-68. https://doi.org/10.1016/j.micromeso.2017.07.028

Zhang, Q., Hou, Q., Huang, G. and Fan, Q. (2020), "Removal of heavy metals in aquatic environment by graphene oxide composites: A review", *Environ. Sci. Pollut. Res.*, **27**, 190-209. https://doi.org/10.1007/s11356-019-06683-w

Zhang, H., Lv, X., Li, Y., Wang, Y. and Li, J. (2010), "P25-graphene composite as a high performance photocatalyst", *ACS Nano.*, **4**, 380-386. https://doi.org/10.1021/nn901221k

Zerrouki, R., Karas, A., Zidour, M., Bousahla, A.A., Tounsi, A., Bourada, F., Tounsi, A.D, Benrahou, K.H. and Mahmoud, S.R. (2021), "Effect of nonlinear FG-CNT distribution on mechanical properties of functionally graded nano-composite beam", *Struct. Eng. Mech.*, **78**(2), 117-124. https://doi.org/10.12989/sem.2021.78.2.117

JL